Available online at www.sciencedirect.com
ScienceDirect
Journal of Molecular Spectroscopy 251 (2008) 56–63
Journal of MOLECULAR SPECTROSCOPY
www.elsevier.com/locate/jms

Reinvestigation of the microwave spectrum of 2-methylmalonaldehyde

Vadim V. Ilyushin [a,b], Eugene A. Alekseev [b], Yung-Ching Chou [c,*], Yen-Chu Hsu [c], Jon T. Hougen [a], Frank J. Lovas [a], Laura B. Picraux [d,1]

[a] Optical Technology Division, NIST, Gaithersburg, MD 20899-8441, USA
[b] Institute of Radio Astronomy of NASU, Chervonopraporna 4, 61002 Kharkov, Ukraine
[c] Institute of Atomic and Molecular Sciences, Academia Sinica, P.O. Box 23-166, Taipei 10617, Taiwan
[d] Chemical Sciences and Technology Laboratory, NIST, Gaithersburg, MD 20899, USA

Received 22 November 2007; in revised form 28 December 2007
Available online 11 January 2008

Abstract

The molecule 2-methylmalonaldehyde (2-MMA) exists in the gas phase as a six-membered hydrogen-bonded ring [HO—CH=C(CH_3)—CH=O] and exhibits two large-amplitude motions, an intramolecular hydrogen transfer and a methyl torsion. The former motion is interesting because transfer of the hydrogen atom from the hydroxyl to the carbonyl group induces a tautomerization in the ring, which then triggers a 60° internal rotation of the methyl group attached to the ring. We present a new experimental study of the microwave spectra of the 2-MMA-d0 [HO—CH=C(CH_3)—CH=O] and 2-MMA-d1 [DO—CH=C(CH_3)—CH=O] isotopologs of the molecule. The new measurements were carried out by Fourier-transform microwave (FTMW) spectroscopy in the 8–24 GHz frequency range and by conventional absorption spectroscopy in the 49–149 GHz range. In the present work, we use a tunneling-rotational Hamiltonian based on a $G_{12}{}^{m}$ group-theoretical formalism to carry out global fits of 2578 2-MMA-d0 transitions and 2552 2-MMA-d1 transitions to measurement uncertainty, obtaining a root-mean-square deviation of 0.015 MHz for both isotopologs. This represents a significant improvement in fitting accuracy over past attempts. Some problems associated with calculating barrier heights from the observed tunneling splittings and assumed tunneling paths are also considered.

Keywords: Hydrogen transfer; Internal rotation; Large-amplitude motion; Microwave spectrum; Tunneling Hamiltonian; Tunneling splittings

1. Introduction

The molecule 2-methylmalonaldehyde (2-MMA) is of interest for molecular spectroscopy because it involves two large-amplitude motions: an intramolecular hydrogen transfer and a methyl-top internal rotation. Fig. 1 shows the equilibrium structure of 2-MMA and the transition state in the tunneling path involving hydrogen transfer. The act of hydrogen transfer induces a tautomeric rearrangement of the C—C, C—O single and double bonds in malonaldehyde, and triggers an extra 60° internal rotation of the methyl group. Therefore, the molecular system under study provides information on two important classes of phenomena in chemical and biochemical reactions: one is the transmission of chemical information via the exchange of single and double bonds; the other is the triggering, by some motion in one part of the molecule, of a different motion in another part of the molecule.

This is the third paper on the microwave spectrum of 2-MMA. Sanders [1] presented the first microwave measurements on this system, discussed the basic theoretical concepts necessary to understand the rotational spectrum of a molecule with these two large-amplitude motions, and derived a number of molecular parameters from his spectrum. Much later, two of the present authors showed [2] that Sanders' data could be fit with much greater precision using a high-barrier tunneling formalism originally

* Corresponding author. Present address: Department of Natural Science, Taipei Municipal University of Education, Taipei 10048, Taiwan.
E-mail address: wavechou@yahoo.com.tw (Y.-C. Chou).
[1] Present address: Rohm and Haas Co., Spring House, PA 19477, USA.

0022-2852/$ - see front matter © 2008 Elsevier Inc. All rights reserved.
doi:10.1016/j.jms.2008.01.005

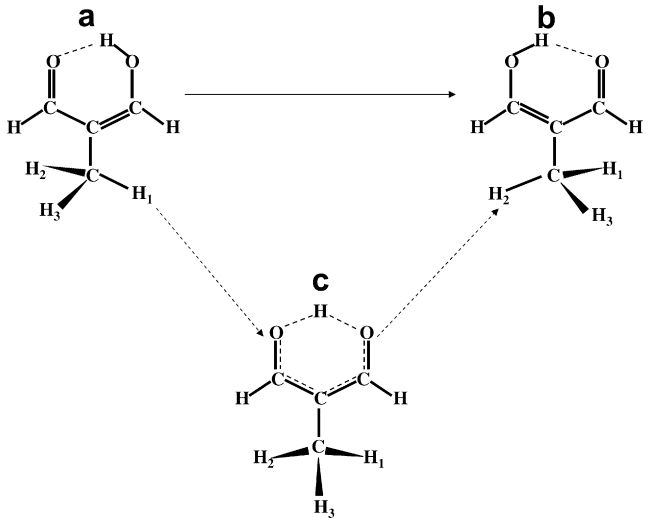

Fig. 1. A sketch of the equilibrium conformations of 2-MMA and the transition state in the tunneling path involving hydrogen transfer and corrective internal rotation. (a) and (b) are two of the six equilibrium conformations of 2-MMA, and (c) is the transition state in the (a) → (b) tunneling path in the group-theoretical formalism. The methyl rotor experiences a 3-fold torsional barrier in the equilibrium conformations (a) and (b) and a 6-fold torsional barrier in the transition state (c).

developed for methylamine. The reader is referred to these two papers for further introductory material and background concerning this problem.

Even though the fit in [2] was quite satisfactory, questions arising from the exclusion of a few of Sanders' measurements from the fit, from the relatively small number of measurements available from Sanders' tables [1], and from the measurement accuracy available at that time, still remained. In the present paper, we have increased the number of measured lines by almost a factor of 30, and increased their frequency range from $14 \leqslant \nu \leqslant 40$ GHz to $8 \leqslant \nu \leqslant 149$ GHz. In addition, the Fourier-transform microwave (FTMW) measurements present a 20-fold improvement in measurement precision, together with a 5-fold improvement given by the millimeter wave measurements. We have also shown that the formalism employed in [2] is capable of fitting these new higher precision measurements to nearly experimental accuracy. This allowed us: (i) to confirm the validity of discarding a few lines from Sanders' tables, (ii) to verify the stability of the molecular constants when more data were added, (iii) to confirm a surprising anomaly in the internal rotation splitting for the normal and singly deuterated species, and (iv) to confirm the validity of the two-dimensional tunneling model for hydrogen transfer and internal rotation to the 10 kHz accuracy level.

2. Experimental

Since 2-MMA is not available commercially, it was necessary to prepare a sample by hydrolyzing the commercially available ester 3-ethoxymethacrolein (C_2H_5—O—CH=C(—CH_3)—CH=O) following one of the two recipes in Sanders' thesis [3]. Ethoxymethacrolein with a stated purity of 96% was purchased from Aldrich [4], and used without further purification. Although the previous hydrolysis recipe [3] passed through a neutralization procedure using NaOH followed by an evaporation-to-dryness isolation of the sodium salt, and reacidification with gaseous HCl, we found it convenient to simply vigorously stir 1 ml of the ethoxymethacrolein with 50 ml of H_2O (or D_2O when the monodeuterated —OD compound was desired) at room temperature for 3–4 h. This seemed to give complete hydrolysis of the ethyl ester linkage, and the 2-MMA product was then isolated as a solid by evaporating the aqueous solution to dryness at room temperature under vacuum. Heating was avoided in the preparation both because of the thermal instability and the volatility of 2-MMA.

Spectra were recorded using a NIST FTMW spectrometer [5] and the Kharkov millimeter wave spectrometer [6]. About 170 new FTMW lines were measured for the d0 species (normal isotopolog) and about 160 for the d1 species (monodeuterated isotopolog with an —OD group), with an estimated measurement precision of 2 kHz for the normal species. (All lines were weighted in our fits by the inverse square of their assigned uncertainties.) The FTMW d1 lines were assigned an uncertainty of 10 kHz, since the blended deuterium quadrupole hyperfine components significantly degrade the measurement precision. (We simply took the center of the broadened lines as the transition frequency.) About 2300 new mm-wave lines for each isotopolog were measured in Kharkov, with an estimated measurement precision of 10 kHz for unblended lines and 50 kHz for blended and weak lines. Finally, lines from Sanders' tables which did not fall in our present measurement ranges were assigned a measurement uncertainty of 50 kHz. The measurements treated in this paper are summarized in Table 1, and given in full as supplementary data (Appendix A).

A particularly important new addition to the data base here was the measurement of 58 b-type transitions for the d0 species and 70 b-types for the d1 species. These transitions are important because they go across the H-transfer tunneling splittings as shown in Fig. 2, and thus represent a direct measure of these splittings. Such transitions were not present in Sanders' data set, where tunneling splitting information was obtained somewhat more indirectly, from perturbations going across the splittings.

3. Theoretical

We use here the Hamiltonian described in detail in [2]. The physical model assumes that the molecule is confined for many vibrations to one of six equilibrium frameworks, but that it occasionally tunnels from one of these six minima to another. This is often referred to as the high-barrier approximation (as opposed to the infinite-barrier approximation, where no tunneling splittings are observed, or the low-barrier approximation, where the present formalism

Table 1
Overview of 2-MMA measurements used in the present work

Lab[a]	Year	Apparatus[b]	Range[c]	d0			d1		
				#[d]	Unc[e]	rms[f]	#[d]	Unc[e]	rms[f]
NIST	2005	FTMW	8–24	176	2	2.5	161	10	9.2
Harvard	1979	Stark	14–40	68	50	48.1	53	50	32.5
Kharkov	2006	mm-wave	49–149	1876	10	11.1	1976	10	11.7
Kharkov	2006	mm-wave	49–149	458	50	21.3	362	50	26.7

[a] The NIST and Kharkhov measurements are from the present work. The Harvard measurements are from Sanders' Ph.D. Thesis work [1,3].
[b] The FTMW and mm-wave spectrometers are described in Refs. [5,6]. The Harvard apparatus was a conventional Stark spectrometer of that era [3].
[c] The frequency range (in GHz) of the measurements in each row.
[d] Number of measured lines included in the fit for the category described at the left of each row, given separately for the normal (OH or d0) and the OD (d1) isotopologs of 2-MMA.
[e] Estimated experimental measurement uncertainties (in kHz), which are then used to determine weights for lines in the fit equal to $1/(\mathrm{unc})^2$. Larger FTMW uncertainties are used for the d1 isotopolog, because of the partially resolved deuterium quadrupole structure. Kharkov lines are divided into unblended (third row) and blended (fourth row).

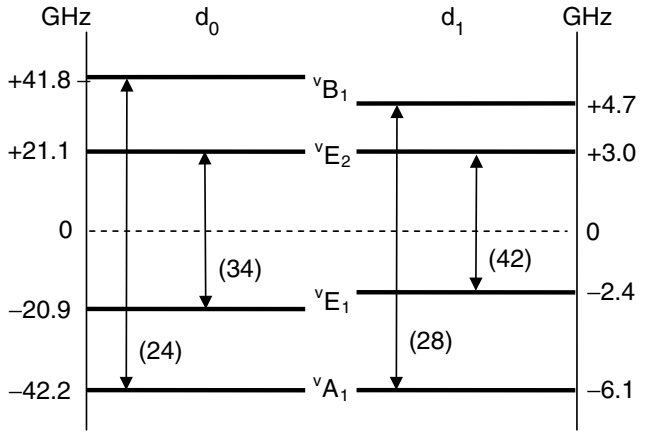

Fig. 2. Schematic illustration of the $J = 0$ inversion–torsion levels of 2-methylmalonaldehyde, as given by Eqs. (5) of [2], and of allowed transitions across the tunneling splittings. (The vast majority of transitions, of course, occur between rotational states within any given inversion–torsion manifold, but they are not indicated in this diagram.) Transitions between nondegenerate and degenerate levels are forbidden, even in the rotating molecule, so no experimental measurements of ^{v}A–^{v}E or ^{v}B–^{v}E splittings can be obtained (similar to the well-known situation in a methyl-top internal rotation problem). On the other hand, as shown in this diagram, transitions between rotational levels of the $^{v}A_1$ and $^{v}B_1$ nondegenerate inversion–torsion manifolds or between rotational levels of the $^{v}E_1$ and $^{v}E_2$ doubly degenerate inversion–torsion manifolds are allowed for 2-methylmalonaldehyde. Numbers in parentheses next to the transition arrows indicate the number of rotational transitions (b-type) across the corresponding tunneling splittings observed in the present work. Such transitions, which clearly help to fix the tunneling splitting parameters, were not observed in Ref. [1].

breaks down). The Hamiltonian is represented as a sum of terms of the form VR, where the vibrational factor V represents an operator containing only the two large-amplitude motions (i.e., the hydrogen transfer coordinate and the internal rotation angle and/or their conjugate momenta), while the rotational factor R represents an operator containing some product of integer powers of molecule-fixed Cartesian components of the total angular momentum operator of the form $J_x^m J_y^n J_z^p$. Group-theoretical and time-reversal arguments are used to determine which products of functions V and R are allowed in the Hamiltonian. For notational purposes we repeat here only Eq. (1) from Ref. [2] (after putting a factor of $\frac{1}{2}$ in front of the last term to correct an omission in [2]):

$$H = h_v + h_j \mathbf{J}^2 + h_k J_z^2 + (f_+ J_+^2 + f_- J_-^2) + qJ_z + (r_+ J_+ + r_- J_-) + (1/2)[s_+(J_+ J_z + J_z J_+) + s_-(J_- J_z + J_z J_-)], \quad (1)$$

and point out that higher order J and K_a dependences of the h, f, q, r, and s parameters are indicated by adding subscripts j and k, e.g., h_v, $h_j\mathbf{J}^2$, $h_k J_z^2$, $h_{jj}\mathbf{J}^4$, $h_{jk}J^2J_z^2$, $h_{kk}J_z^4$, etc. We further note that each of the fitting constants (i.e., each of the letters h, f, q, r, s) will also acquire an additional subscript $n = 1$–6, which indicates that they represent Hamiltonian matrix elements associated with no tunneling ($n = 1$) or tunneling from framework 1 to framework $n > 1$. The reader is referred to [2] and references therein for a much more detailed description of this formalism.

The fitting program used here was essentially that obtained from Ohashi [7] and used in our earlier work [2], except that some modifications were made to permit location of eigenvectors and eigenvalues with the correct J and K quantum numbers after the large matrix diagonalizations necessary for high J levels. The symmetry species of the symmetric-top rotational basis functions given in Table 1 of Ref. [2] allow one to determine the $^{r}A_1$, $^{r}A_2$, $^{r}B_1$, $^{r}B_2$ symmetry species sequence for the asymmetric-rotor J_{K_a,K_c} levels from $J_{0,J}$ to $J_{J,0}$ for any given J. Figs. 2 and 3 indicate that the vibrational symmetry species of tunneling components in the zero-point vibrational level of 2-MMA are $^{v}A_1$, $^{v}E_1$, $^{v}E_2$, and $^{v}B_1$. For nondegenerate vibration-rotation levels of given J we thus expect two $^{vr}\Gamma$ symmetry species sequences, each containing $2J + 1$ levels: one will be identical to the $J_{K_aK_c}$ species sequence found in Table 1 of Ref. [2], corresponding to the rotational levels of the $^{v}A_1$ vibrational state; the other will be equal to the $J_{K_aK_c}$ species sequence found in Table 1 of Ref. [2] multiplied by B_1, corresponding to the rotational levels of the $^{v}B_1$ vibrational state. The labeling procedure first deter-

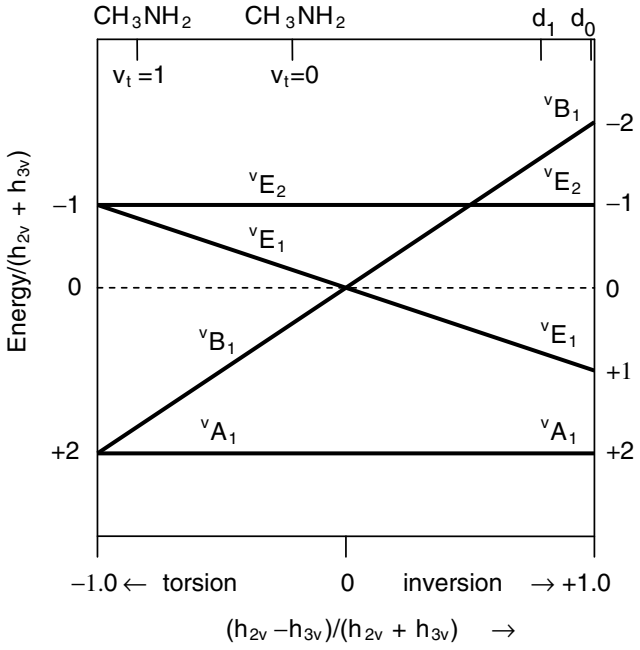

Fig. 3. Schematic illustration of inversion–torsion energy level splittings according to Eqs. (5) of [2]. The diagram has been drawn with unitless abscissa and ordinate, obtained by dividing both scales by $h_{2v} + h_{3v}$. At the pure torsional splitting limit, shown on the left ($h_{2v} = 0$), the unitless energy levels consist of two superimposed nondegenerate levels at +2 separated from two doubly degenerate levels at −1. At the limit of only H-transfer plus corrective internal rotation splittings, shown on the right ($h_{3v} = 0$), the unitless energy levels consist of a benzene-π-orbital-like pattern, with the two nondegenerate levels at the bottom and top (at ±2), and the doubly degenerate levels in between (at ±1). At the center, where the inversion and torsion splitting parameters are equal ($h_{2v} - h_{3v} = 0$), the lowest level is nondegenerate (at +2), the highest is doubly degenerate (at −1), and the middle level is accidentally triply degenerate (at 0). Markers at the top of the diagram indicate positions along the abscissa appropriate for 2-methylmalonaldehyde-d0 and -d1, as well as positions appropriate for the first two torsional levels of methylamine [8,9]. Note that the unitless energies in this figure must be multiplied by $h_{2v} + h_{3v}$, and that the values of these two parameters can be either positive or negative [8,9].

mines the particular vibrational state to which the eigenvectors belong (e.g., $^{v}A_1$ or $^{v}B_1$ for nondegenerate vibration-rotation species), and then assigns J_{K_a,K_c} labels by comparison with the $^{vr}\Gamma$ symmetry species sequences for that vibrational state. Consider for example the $^{vr}A_1$ vibration-rotation symmetry block, which contains product basis functions of only two types: $^{v}A_1{}^{r}A_1$ and $^{v}B_1{}^{r}B_1$. Following the procedure described above we assigned a $^{v}A_1$ or $^{v}B_1$ dominant vibrational symmetry to each eigenvector (i.e., each eigenvector was assigned to the $^{v}A_1$ or $^{v}B_1$ vibrational level) by comparing the sum of squared coefficients in each eigenfunction for vibrational basis functions of $^{v}A_1$ symmetry with the corresponding sum for vibrational basis functions of $^{v}B_1$ symmetry. The levels obtained in this way for the $^{v}A_1$ (or $^{v}B_1$) vibrational tunneling component were then ordered in increasing energy, and J_{K_a,K_c} labels were assigned by comparison with the $^{r}A_1$ (or $^{r}B_1$) positions in the asymmetric-rotor symmetry species sequence determined for given J from Table 1 of Ref. [2]. The same procedure was used for the $^{vr}A_2$, $^{vr}B_1$, and $^{vr}B_2$ vibration-rotation symmetry blocks. Treatment of the $^{vr}E_1$ and $^{vr}E_2$ symmetry blocks was similar, except that each block contains four types of product basis functions, e.g., $^{vr}E_1$ contains $^{v}E_1{}^{r}A_1$, $^{v}E_1{}^{r}A_2$, $^{v}E_2{}^{r}B_1$, and $^{v}E_2{}^{r}B_2$.

A qualitative understanding of the competition between inversion tunneling (our shorthand term for the hydrogen-transfer motion plus corrective internal rotation [2]) and pure torsional tunneling in determining the tunneling splitting pattern in 2-MMA can be obtained from Fig. 3, which illustrates the $J = 0$ energy levels calculated from Eqs. (5) of [2]. Those equations include only the two main tunneling splitting parameters, h_{2v} and h_{3v}, where h_{2v} is associated with the inversion motion and h_{3v} is associated with the pure internal rotation. In the inversion–torsion vibrational ground state, both are negative. Fig. 3 actually plots energy levels divided by $h_{2v} + h_{3v}$, which makes it easier to follow the change in splitting pattern from the left of the diagram, where only pure internal rotation occurs, to the right, where only hydrogen-transfer plus corrective internal rotation occurs. It is interesting to note, as indicated at the top of Fig. 3, that the two isotopologs of 2-MMA studied here, together with the ground and first excited torsional states of methylamine studied earlier [8,9], provide examples of four different regimes in this diagram. For example, the first torsional state of methylamine and the normal isotope of 2-MMA represent the two limiting cases, i.e., $|h_{2v}| << |h_{3v}|$ (torsional splitting dominates) and $|h_{2v}| >> |h_{3v}|$ (inversion splitting dominates), while the ground state of methylamine has $|h_{2v}| \approx |h_{3v}|$ (both splittings comparable). Clearly, the large-amplitude motion splitting pattern for molecules of the type considered here depends on the potential surface, on the location of any deuteration, and on the number of quanta found in the torsional and inversion modes.

4. Spectral fits

A least squares fit of 2578 transitions in 2-MMA-d0 to 37 parameters was carried out, giving a root-mean-square deviation of 0.015 MHz. A copy of the fitting program, and the input and output files are deposited in supplementary material (Appendix A). The molecular parameters from this fit are shown in Table 2, where parameters from our earlier fit of only Sanders' data are shown for comparison.

A least squares fit of 2552 transitions in 2-MMA-d1 to 32 parameters was also carried out, using the same program as for the d0 species. This fit again gave a root-mean-square deviation of 0.015 MHz. The input and output files for the d1 species are deposited in the supplementary material. The molecular parameters are shown in Table 3, where parameters from our earlier fit of Sanders' data are again shown for comparison.

The fits for both isotopologs are excellent. In particular, the root-mean-square deviations given in Table 1 demonstrate that our new measurements are quite accurate and

Table 2
Molecular parameters[a] from least-squares fits of tunneling-rotational transitions[b] in the ground vibrational level of 2-methylmalonaldehyde-d0

	This work	Ref. [2]		This work	Ref. [2]
$A-\overline{B}$	2236.84780(25)	2236.792(25)	r_2	−28.748(59)	
$\overline{B}$	2801.135314(84)	2801.1761(36)	$r_{2j}\times10^3$	0.0612(47)	
$(B-C)/4$	353.491836(42)	353.5113(12)	h_{4v}	9.30569(64)	8.98(45)
s_1	29.3832(44)	31.516(12)	h_{4k}	0.000981(20)	
ρ	0.0319219050(54)	0.0319274(19)	f_4	0.0000275(16)	
$D_J\times10^3$	0.329303(25)	0.201(42)	r_4	−0.02068(56)	
$D_{JK}\times10^3$	0.73322(16)	1.17(19)			
$D_K\times10^3$	3.87343(43)	7.84(61)	h_{3v}	−111.4925(59)	−111.10(58)
$\delta_J\times10^3$	−0.095933(12)		h_{3j}	−0.0007446(54)	
$\delta_K\times10^3$	−0.359057(83)		h_{3k}	−0.044456(47)	
$s_{1J}\times10^3$	−0.12294(32)		f_3	0.0023217(22)	
$s_{1K}\times10^3$	0.35013(39)		$h_{3kk}\times10^3$	−0.00448(28)	
$\rho_J\times10^6$	−0.037797(55)		$f_{3k}\times10^3$	−0.001046(53)	
$\rho_K\times10^6$	−0.01454(21)		r_3	0.26051(28)	
			$r_{3j}\times10^3$	−0.01122(45)	
h_{2v}	−21013.0064(14)	−21010.86(62)	$r_{3k}\times10^3$	0.0348(24)	
h_{2j}	0.04473(16)	0.00544(85)	h_{5v}	−0.0643(33)	
h_{2k}	1.76358(16)	1.7895(65)			
f_2	−0.126349(80)	−0.10699(37)			
$h_{2jj}\times10^3$	−0.000290(24)		# of lines[c]	2578	88
$h_{2kk}\times10^3$	−0.06167(26)		rms	0.015	0.12
$f_{2k}\times10^3$	−0.031385(53)				

[a] Numbers in parentheses denote one standard deviation (type A, $k=1$) [10] and apply to the last digits of the parameters. All parameters and the root-mean-square deviation (rms) of the fit are in MHz, except for ρ, ρ_J, and ρ_K, which are unitless.
[b] The transition frequencies used are summarized in Table 1.
[c] Number of transitions included in the fit.

Table 3
Molecular parameters[a] from least-squares fits of tunneling-rotational transitions[b] in the ground vibrational level of 2-methylmalonaldehyde-d1

	This work	Ref. [2]		This work	Ref. [2]
$A-\overline{B}$	2253.9162(38)	2253.681(20)	f_2	−0.016850(58)	−0.01800(70)
$\overline{B}$	2755.7806(13)	2755.8107(33)	$f_{2j}\times10^3$	0.0000726(67)	
$(B-C)/4$	344.59585(63)	344.6029(14)	$f_{2k}\times10^3$	−0.001750(72)	
s_1	47.062(42)	48.3216(52)	r_2	−2.132(72)	
ρ	0.03180863(39)	0.0317978(81)	s_2	0.001639(77)	
$D_J\times10^3$	0.310121(42)	0.277(41)	h_{4v}	1.76648(52)	
$D_{JK}\times10^3$	0.80161(42)		f_4	0.0000123(17)	
$D_K\times10^3$	3.5076(10)		h_{6v}	−0.3066(63)	
$\delta_J\times10^3$	−0.088772(21)				
$\delta_K\times10^3$	−0.38492(23)		h_{3v}	−348.2129(71)	−348.95(30)
$s_{1J}\times10^3$	−0.10294(96)		h_{3j}	−0.0005759(61)	
$s_{1K}\times10^3$	0.3727(44)		f_3	−0.0003105(27)	
$\rho_J\times10^6$	−0.0136(11)		$f_{3k}\times10^3$	−0.001879(57)	
$\rho_K\times10^6$	−0.1389(25)		r_3	0.2602(10)	
			s_3	0.00269(12)	
h_{2v}	−2695.5740(60)	−2693.84(30)	h_{5v}	0.3314(33)	
h_{2j}	0.00619(11)				
h_{2k}	0.27878(16)	0.279(12)	# of lines[c]	2552	75
			rms	0.015	0.10

[a] Numbers in parentheses denote one standard deviation (type A, $k=1$) [10] and apply to the last digits of the parameters. All parameters and the root-mean-square deviation (rms) of the fit are in MHz, except for ρ, ρ_J, and ρ_K, which are unitless.
[b] The transition frequencies used are summarized in Table 1.
[c] Number of transitions included in the fit.

that the hydrogen-transfer–internal-rotation tunneling Hamiltonian used here is capable of describing energy levels and their splittings to 10 kHz.

The constants in Tables 2 and 3 are organized as follows. Those in the first column with no numerical subscript or the subscript 1 refer to quantities characterizing the non-tunneling molecule. The first five rows contain parameters related to the equilibrium structure of the molecule, namely: linear combinations of the usual rotational constants A, B, and C; a coefficient s_1 (see Eqs. (1)–(7) of

[9]), which is an off-diagonal component of the 3 × 3 rotational constant matrix; and the quantity ρ, which is a ratio of the moment of inertia of the methyl group about its symmetry axis to a (nonprincipal) moment of inertia of the whole molecule (see Eqs. (10) of [11]) and is a close analog of the same quantity in ordinary internal rotation problems. It can be seen from Tables 2 and 3 that these parameters change by very small amounts when the number of transitions in the fit is increased by a factor of approximately 30, indicating that no major change has occurred in our understanding of the molecular structure. Many of the various centrifugal distortion terms of these five quantities given in the next nine rows could not be determined from Sanders' data set, so no comparison with results from [2] is possible. All of these centrifugal distortion constants are small, suggesting that the chemical bonds in the nontunneling equilibrium structure can be considered to have a "normal" degree of rigidity with respect to distortion by centrifugal forces.

The next set of molecular parameters, all of which have an even numerical subscript $n = 2$, 4, or 6, characterize the hydrogen-transfer plus corrective internal rotation tunneling motion. In particular, the subscripts 2, 4, and 6 characterize, respectively, energy splitting contributions arising because of tunneling in this large-amplitude motion from a given potential minimum (i.e, a given configuration) to its nearest-neighbor, next-nearest-neighbor, and next-next-nearest-neighbor minima (see Fig. 2 of our earlier paper [2] for a diagram of these minima). For the high-barrier tunneling approximation (used to derive the present formalism) to be valid, it is required that $|h_{2v}| >> |h_{4v}| >> |h_{6v}|$. It can be seen that $|h_{2v}|/|h_{4v}| \approx 2000$ for both isotopologs. The relatively large value of $|h_{6v}|$ for the d1 species may be an artifact caused by the known tendency for the last term in the parameter expansion describing a given physical phenomenon to be strongly contaminated by contributions from a number of extraneous higher-order effects not treated properly by the truncated Hamiltonian. It can be seen that the nearest-neighbor tunneling parameter h_{2v} is almost unchanged from Ref. [2] when the present data set is used. Of some interest is the r_2 term, determined for the first time here. This term describes a $\Delta K = \pm 1$ Coriolis interaction between angular momentum generated by the hydrogen-transfer plus corrective internal rotation motion and the overall angular momentum (see Eqs. (1) and (8)–(12) of [9]) and could be determined here because of the high precision of our new measurements.

The final set of molecular parameters in Tables 2 and 3 all have an odd numerical subscript greater than unity, i.e., $n = 3$ or 5. These subscripts label terms characterizing nearest-neighbor and next-nearest-neighbor tunneling in the pure internal rotation motion (see Fig. 2 of [2]). We again conclude that the high-barrier approximation is applicable to this motion, since $|h_{3v}| >> |h_{5v}|$ is satisfied. The most important conclusion from this part of Tables 2 and 3 is that the unexpected 3-fold increase in internal rotation tunneling splitting upon deuteration of the OH group found in [2] is completely confirmed by the fits to our much larger and much more precise data sets. The implications of this for the 3-fold internal rotation barrier determination are discussed in the following section.

5. Barrier heights from observed tunneling splittings and assumed tunneling paths

5.1. Barrier to the pure torsional large-amplitude motion (LAM)

The quantity $|3h_{3v}|$ corresponds, as shown on the left of Fig. 3, to the usual E–A internal rotation splitting in a methyl-top molecule. This observed quantity can thus be combined with a calculated value for the internal rotation parameter F to obtain a barrier height from the usual internal rotation Hamiltonian

$$H = T + V = Fp_\alpha^2 + (1/2)V_n(1 - \cos n\alpha), \quad (2)$$

where α is the internal rotation angle and $n = 3$ for the methyl torsion. We have calculated values for the principal-axis rotational constants A_P, B_P, C_P, for the moment of inertia of the top about its symmetry axis I_α, and for F from the first five fitting parameters in Table 2. Principal-axis rotational constants $A_P = 5038.5473(3)$, $B_P = 3507.5548(1)$, $C_P = 2094.1516(1)$, and the direction cosines of the top axis $\lambda_z = 0.99982$, $\lambda_x = -0.01920$ in the principal-axis system can be obtained by diagonalizing the rotational constant matrix from Table 2, using s_1 as the coefficient of $(J_zJ_x + J_xJ_z)$. Substituting these values and ρ (or their analogs for the OD species) into some of Eqs. (2–25) and (2–30) in Ref. [12] then yields values for F of 5.43806 and 5.42629 cm^{-1} for 2-MMA-d0 and 2-MMA-d1, respectively, as well as values for I_α of 3.2022 and 3.2087 uÅ^2. These values for I_α lie in the normal range and thus support the validity of this procedure.

As expected, the calculated value of F is nearly invariant to deuteration of the hydroxyl group in 2-MMA, but the large difference in fitted h_{3v} values in Tables 2 and 3 leads to rather different barrier heights, namely:

$$V_3(\mathrm{OH}) = 400.7\ \mathrm{cm}^{-1}$$
$$V_3(\mathrm{OD}) = 311.6\ \mathrm{cm}^{-1}. \quad (3)$$

Uncertainties cannot be given, since we have fit one unknown, $3h_{3v}$, to one parameter, V_3. This 89 cm^{-1} decrease in effective barrier height after deuteration of the hydroxyl group is quite large and somewhat surprising. Furthermore, both of these values are higher than the 240 cm^{-1} calculated value given in Fig. 4 of Ref. [13], but those authors indicate that their barrier values are dependent on the computational methods used, and in particular the DFT method used in their work underestimates barrier values [13].

No convincing explanation for the large observed change in h_{3v} upon deuteration presented itself during our earlier work [2], but the rather small data set provided

by Sanders' measurements left open the possibility that the large change might have been caused by one or more misassignments in our earlier data set. The present data set is almost 30 times larger, however, and the fit is excellent, so we now believe that the fitted values of h_{3v} presented in Tables 2 and 3 (which are essentially the same as our earlier values) are the correct ones for the present high-barrier tunneling model.

One explanation for this 89 cm^{-1} change is to ascribe it to "unknown model error", where, for example, some fraction of the 100 times larger h_{2v} hydrogen-transfer tunneling frequency (in the OH isotopomer) contributes in an unsuspected way to the fitted h_{3v} tunneling frequency. This explanation is supported by the fact that we are unable to explain the H/D isotope dependence of the tunneling splitting for the H-transfer LAM (see discussion below).

Another explanation involves postulating: (i) a 600 cm^{-1} increase in the O—H stretching frequency when going from the equilibrium configuration at the bottom of the internal rotation well (where the O—H stretch is presumably strongly red-shifted by the intramolecular hydrogen bond) to the top of the barrier, and (ii) a $1/\sqrt{2}$ shift in both vibrational frequencies for the OD species. The change in zero-point contribution from this small-amplitude vibration to the "vibrationally averaged" internal rotation barrier would then approximate the desired 89 cm^{-1}. This explanation (or some more elaborate version of zero-point energy differences and/or vibrational averaged structures for the OH and OD groups at the top and bottom of the barrier) could presumably be tested by high-level ab initio calculations.

5.2. Barrier to the H-transfer LAM

It is less straightforward to go from the observed h_{2v} values in Tables 2 and 3 to effective barrier heights for the hydrogen-transfer plus corrective internal rotation motion. We initially hoped to obtain a barrier height by treating the H-transfer LAM as a one-dimensional mathematical problem after parameterizing: (i) the tunneling path itself, (ii) the potential along this path, and (iii) the effective mass moving along this path. Such an approach is quite appealing, since the tunneling model used here to obtain a near-quantitative fit to the experimental data essentially assumes that the system point travels, for each large-amplitude tunneling motion, along some path (i.e., along some line) in coordinate space which does not intersect the path of any other large-amplitude tunneling motion (as illustrated schematically, for example, in Fig. 4 of [14]). Even though our one-dimensional approach was not successful, we describe a few results below, since they lead rather naturally to the conclusion that a two-dimensional approach will be necessary.

Note that we use the phrase "one-dimensional mathematical problem" here to denote motion involving one position coordinate and one momentum conjugate to that position. Thus, any motion describable by the position and velocity of the system point on a specified curve in multi-dimensional space is considered to be one-dimensional, no matter how many chemical bonding dimensions (e.g., stretches, bends, torsions, inversions, etc.) that specified curve may sample. Similarly, we use the phrase "two-dimensional mathematical problem" to denote motion involving two position coordinates and two conjugate momenta. Thus any motion describable by the position and velocity of the system point on a specified two-dimensional surface in multi-dimensional space is considered to be two-dimensional, no matter how many chemical dimensions the surface may sample.

The H-transfer LAM was treated as a 6-fold periodic-well problem involving motion along a single coordinate angle β, with the further assumption that the potential energy along the path can be expanded as a rapidly convergent Fourier series. The Hamiltonian is then given by Eq. (2) with α replaced by β and $n = 6$. The parameter F in Eq. (2) is no longer a constant, but a Fourier series for its variation with β can be calculated from estimates of the effective mass at each point along the path. As mentioned, our one-dimensional approach was not successful, so we give below only the main qualitative results.

When the H-transfer motion plus corrective internal rotation is considered to involve the motion of four H atoms along the tunneling path (i.e., one from the OH and three from the CH_3), then the effective mass is essentially 4 for the OH species and 5 for the OD species, and we find values of V_6 for the two isotopologs of a few hundred wavenumbers (cm^{-1}). These values are much smaller than expected and differ from each other by nearly a factor of two. When the H-transfer motion plus corrective internal rotation is arbitrarily considered to involve the motion of only one H atom along the tunneling path (i.e., that of the OH group), then the effective mass is essentially 1 for the OH species and 2 for the OD species, and we find values of V_6 for the two isotopologs that are much larger (a few thousand wavenumbers (cm^{-1})) and in remarkably good agreement with each other.

The results above seem to suggest that the corrective internal rotation of the methyl group is somehow or other not part of the tunneling process. Such an idea can be rationalized intuitively by imagining that the hydroxyl H and the single ↔ double bond rearrangements first proceed to the midpoints of their respective tunneling paths, where the 3-fold barrier to internal rotation vanishes by symmetry. At this point the corrective internal rotation of the methyl group takes place against only the resistance of a small 6-fold barrier (almost no tunneling barrier; see Fig. 1). Once the corrective internal rotation has been completed, the hydroxyl H and the single ↔ double bond rearrangements proceed to the end points of their respective tunneling paths. This intuitive approach leads, however, to the somewhat unappealing requirement that the potential energy V, as a function of distance along the angle β, is large when the H-transfer motion is occurring, but that

it decreases suddenly to a small value just before the corrective internal rotation occurs.

Looking at things from a time-domain point of view, Ushiyama and Takatsuka [13] concluded from ab initio trajectory calculations that the hydrogen transfer, double–single bond exchange, and internal rotation do not proceed simultaneously, but in fact proceed nearly sequentially, with the internal rotation motion lagging significantly behind the hydrogen transfer. (Our computational model above actually corresponds to the opposite case, where all structural changes proceed simultaneously and at constant velocity.) The behavior predicted by Ushiyama and Takatsuka cannot easily be modeled as a traditional one-dimensional quantum mechanical tunneling problem, since the molecular configuration (in particular the methyl torsional angle) at a point on the tunneling path A ↔ B near the equilibrium structure A will be different, depending on whether the system has just departed from A (CH_3 group still at its equilibrium orientation for A) or is just about to arrive at A (CH_3 group still at its equilibrium orientation for B). In more mathematical terms, the molecular configuration is not uniquely defined by the value of the coordinate β at any given point along such a tunneling path; it is also necessary to know the sign of the velocity $d\beta/dt$ at that point.

Since the intuitive picture of "hiding some of the mass from the tunneling motion" cannot easily be achieved in a one-dimensional model, a two-dimensional model seems more promising. One could then in principle apportion the kinetic and potential energies between the two degrees of freedom in such a way that the internal rotation degree of freedom sees almost none of the potential energy (barrier) while the H-transfer degree of freedom sees almost all of it. A careful treatment of such a model is beyond the scope of this work.

6. Summary

An excellent fit to a large body of precise microwave data has been achieved here for 2-methylmalonaldehyde using a group-theoretically derived two-dimensional tunneling Hamiltonian. In spite of this, a precise interpretation of the tunneling parameters from the fit in terms of features of the potential surface has not been achieved. Experimentally, it would obviously be helpful to get high quality measurements for both the OH and OD variants of the CD_3 species. Theoretically, even more remains to be done, including ab initio calculations for the most interesting regions of the potential surface as well as algebraic and numerical investigations of tunneling splittings in problems with simplified model potentials.

Acknowledgment

The author Y.-C.C. thanks the National Science Council of Taiwan, Grant No. NSC 96-2113-M-133-001-MY2 for support.

Appendix A. Supplementary data

Supplementary data for this article are available on ScienceDirect (www.sciencedirect.com) and as part of the Ohio State University Molecular Spectroscopy Archives (http://library.osu.edu/sites/msa/jmsa_hp.htm). Supplementary data associated with this article can be found, in the online version, at doi:10.1016/j.jms.2008.01.005.

References

[1] N.D. Sanders, J. Mol. Spectrosc. 86 (1981) 27–42.
[2] Y.-C. Chou, J.T. Hougen, J. Chem. Phys. 124 (2006) 074319-1-10.
[3] N.D. Sanders, Ph.D. Thesis, Harvard University, 1979.
[4] Certain commercial products are identified in this paper in order to specify adequately the experimental or theoretical procedures. In no case does such identification imply recommendation or endorsement by the National Institute of Standards and Technology, nor does it imply that the products are necessarily the best available for the purpose.
[5] R.D. Suenram, J.U. Grabow, A. Zuban, I. Leonov, Rev. Sci. Instrum. 70 (1999) 2127–2135.
[6] R.A. Motiyenko, E.A. Alekseev, S.F. Dyubko, F.J. Lovas, J. Mol. Spectrosc. 240 (2006) 93–101.
[7] N. Ohashi, Private communication.
[8] N. Ohashi, K. Takagi, J.T. Hougen, W.B. Olson, W.J. Lafferty, J. Mol. Spectrosc. 126 (1987) 443–459.
[9] N. Ohashi, S. Tsunekawa, K. Takagi, J.T. Hougen, J. Mol. Spectrosc. 137 (1989) 33–46.
[10] B.N. Taylor, C.E. Kuyatt, NIST Technical Note No. 1297 (1994). This publication may be downloaded from http://physics.nist.gov/Pubs/guidelines/contents.html.
[11] N. Ohashi, J.T. Hougen, J. Mol. Spectrosc. 121 (1987) 474–501.
[12] C.C. Lin, J.D. Swalen, Rev. Mod. Phys. 31 (1959) 841–892.
[13] H. Ushiyama, K. Takatsuka, Angew. Chem. Int. Ed. 44 (2005) 1237–1240.
[14] J.T. Hougen, J. Mol. Spectrosc. 114 (1985) 395–426.